**ENSO Bred Vectors in Coupled Ocean-Atmosphere General Circulation Models**

S-C Yang[1], M. Cai*[2], E. Kalnay[1], M. Rienecker[3], G. Yuan[4] and Z. Toth[5]

[1] Department of Meteorology, University of Maryland,
College Park, Maryland 20742.

[2] Department of Meteorology, Florida State University,
Tallahassee, Florida 32306

[3] Global Modeling and Assimilation Office, NASA/GSFC,
Greenbelt, Maryland 20770

[4] Bauer Center for Genomics Research
7 Divinity Ave., Harvard University
Cambridge, MA 02138

[5] Environmental Modeling Center, National Centers for Environmental Prediction, NOAA,
Camp Springs, Maryland 20746

*Corresponding author: Dr. Ming Cai, Department of Meteorology, Florida State University, Tallahassee, FL 32306, U.S.A. E-mail: cai@met.fsu.edu

## Abstract

The breeding method has been implemented in the NASA Seasonal-to-Interannual Prediction Project (NSIPP) Coupled General Circulation Model (CGCM) with the goal of improving operational seasonal to interannual climate predictions through ensemble forecasting and data assimilation. The coupled instability as captured by the breeding method is the first attempt to isolate the evolving ENSO instability and its corresponding global atmospheric response in a fully coupled ocean-atmosphere GCM. Our results show that the growth rate of the coupled bred vectors (BV) peaks at about 3 months before a background ENSO event. The dominant growing BV modes are reminiscent of the background ENSO anomalies and show a strong tropical response with wind/SST/thermocline interrelated in a manner similar to the background ENSO mode. They exhibit larger amplitudes in the eastern tropical Pacific, reflecting the natural dynamical sensitivity associated with the presence of the shallow thermocline. Moreover, the extratropical perturbations associated with these coupled BV modes reveal the variations related to the atmospheric teleconnection patterns associated with background ENSO variability, e.g. over the North Pacific and North America. A similar experiment was carried out with the NCEP/CFS03 CGCM. Comparisons between bred vectors from the NSIPP CGCM and NCEP/CFS03 CGCM demonstrate the robustness of the results.

Our results strongly suggest that the breeding method can serve as a natural filter to identify the slowly varying, coupled instabilities in a coupled GCM, which can be used to construct ensemble perturbations for ensemble forecasts and to estimate the coupled background error covariance for coupled data assimilation.

## 1. Introduction

Of all the seasonal-interannual climate variabilities, the El Nino-Southern Oscillation (ENSO) phenomenon plays one of the most important roles in dominating interannual sea surface temperature (SST) variability in the tropical Pacific. Feedbacks through strong atmosphere-ocean coupling in tropics characterize the co-variability of wind, SST and thermocline (or warm water volume) of ENSO, which induces not only a global impact in climate anomalies but also modifies the frequency of extreme weather events like floods or hurricanes. The delayed oscillator mechanism related to tropical waves propagating downwelling/upwelling information in the upper ocean (Schopf and Suarez 1987; Suarez and Schopf 1988; Battisti 1988) can explain many features of ENSO. Jin (1997) further emphasized the importance of the variations of warm water volume in the upper ocean with a warm water recharge/discharge mechanism. It has been shown that the coupled dynamic/thermodynamic mechanisms, i.e., the thermocline and Ekman feedbacks, responsible for delayed or recharge/discharge oscillators, can explain both the west-east asymmetry in the climate mean state and the ENSO variability in the equatorial Pacific basin (Cai 1995; Jin 1996; Dijkstra and Neelin 1999; Van der Vaart et al. 2000; and Cai 2003). Those studies point to the essential role of oceanic memory associated with oceanic wave dynamics. Through the SST that serves as the lower boundary of atmosphere, the oceanic memory dominates the atmospheric seasonal-interannual variability. Therefore, being able to estimate seasonal-interannual variations of SST becomes a crucial factor for successfully predicting seasonal-interannual variability like ENSO. In order to accurately describe the SST and its uncertainties, it is necessary to consider variations of subsurface temperature since they are intimately related to SST

through thermocline feedback and Ekman-layer dynamics.

In the last two decades, ENSO prediction skill with dynamical models has been steadily improving due to the establishment of the tropical observation network, especially the TAO/TRITON mooring arrays, and a better representation of air-sea interaction processes in coupled ocean-atmosphere models. The Zebiak and Cane model, an intermediate coupled ocean-atmosphere model (Zebiak and Cane 1987, hereafter ZC), has been widely used for ENSO studies. However, the presence of errors in the initial conditions limits the forecast performance (Latif et al. 1998). More sophisticated initialization methods have been shown to be important in improving ENSO prediction. For example, data assimilation schemes and ensemble forecasts provide some information on the uncertainties embedded in the initial conditions (Chen et al. 1995, Rosati et al. 1997 and Ballabrera et al. 2000). Recently, Chen et al. (2004) demonstrated that the retrospective forecast from the latest version of this model, due to an improvement of the data assimilation to the ZC model, can have a good skill up to two-year. They also argued that the evolution of El Nino is controlled to a large degree by self-sustaining internal dynamics, suggesting that model-based predictions of El Nino depend more on the oceanic initial conditions rather than on unpredictable atmospheric noise.

Several operational forecast centers around the world now use a coupled general circulation model (CGCM) to forecast ENSO events with an average lead-time around six months. A summary of ENSO forecasts from different operational centers can be found under http://iri.columbia.edu/climate/ENSO/currentinfo/. Current ensemble forecasts are based on one of two approaches for the initialization process: the "two tier"

and the "one tier" configuration (i.e., double or single stage configuration). In the widely used two-tier system, a single forecast of SST anomalies is used to generate an ensemble of atmospheric forecasts (Bengtsson et al. 1993). Since it neglects the coupled nature of the initial perturbations, this approach does not project the ENSO mode on those perturbations. This hardly seems optimal to for seasonal and interannual prediction. The one tier or single stage configuration of CGCM introduced by European Centre for Medium-Range Weather Forecasts (ECMWF) (Stockdale et al. 1998) generates all the ensemble forecasting members via a coupled ocean-atmospheric model in order to have the perturbation growing under a coupled configuration. The NSIPP forecast ensemble, also a one-tier system, includes perturbations in both the atmosphere and ocean, but the initial perturbations are generated independently. Although coupled instabilities will eventually develop in these one-tier systems, they still handicapped by *not including coupled uncertainties in the initial perturbations for ensemble predictions*. Therefore, there is a need for ensemble ENSO prediction systems to include coupled initial perturbations and feedbacks.

The breeding method (Toth and Kalnay 1993, 1997) and singular vectors (Errico and Vukicevic 1992; Buizza and Palmer 1995; and Palmer et al. 1998) are two of the main methods used operationally for generating effective ensemble members in ensemble forecasts with an atmospheric GCM model. Studies of the growth of error/growing modes related with coupled ocean/atmosphere instabilities have generally focused on obtaining singular vector (SV) from a linear/adjoint propagator of intermediate models (e.g., the ZC model). Chen et al. (1997) showed that the error growth depends on the phases of the ENSO and the seasonal cycles, even though initial and final SVs are

insensitive to both. It should be pointed out that their analysis was done using the linear propagator with SST perturbations only, neglecting the coupled nature of the perturbations of other variables. Xue et al. (1997 a,b) used a reduced EOF space spanning the ZC solutions in order to be able to compute the SV for all model variables in a full tangential linear ZC model. They showed that the growth rate and singular vectors are similar to Chen et al. (1997) when choosing an SST norm. However, with an energy norm, the wind and thermocline fields become more important than the SST. Fan et al. (2000) found that SST plays a very important role in seasonal (3-6 months) predictability, and pointed out that using the analysis error covariance as a norm in calculating SV yields quite different results than the frequently used energy norm. The strong dependence of singular vectors on the choice of norm (i.e., the definition of the "size" whose growth is to be maximized) and the choice of optimization time, become limitations when applying this method to a complex system like CGCMs because of existence of various types of instabilities over a whole spectrum of scales. It is difficult to cleanly separate these modes and to keep the coupled instability as the dominant growing mode, since the adjoint model, being linear, can be swamped by the presence of much faster growing atmospheric and oceanic instabilities (Peña and Kalnay, 2004).

Toth and Kalnay (1996) suggested applying the breeding method in a coupled ocean-atmosphere system to isolate ENSO coupled instabilities. The bred perturbations are a superposition of the leading Lyapunov vectors (dominant instabilities) in the dynamical system and the advantages of this method are that it is simple, efficient and independent of the choice of norm. Cai et al. (2003) first tested the breeding method in a coupled system using the ZC model. They found that bred vectors are capable of

describing the characteristics of coupled instabilities associated with the ENSO development. They found that the growth rate is weakest at the peak time of the ENSO states (both positive and negative) and strongest between the events. Unlike the singular vectors, the coupled bred vectors are insensitive to the choice of norm and very sensitive to the background ENSO phase and the time of the year. Their results also suggest that the presence of the "spring-barrier" in the ENSO prediction skill is related to the coupled instability. Filtering out the coupled bred mode from initial perturbations greatly increases the time for doubling forecast error and reduces the "spring-barrier". They also found that using a pair of plus/minus bred vectors as ensemble perturbations led to a significant improvement in the ensemble mean forecast. These results illustrate the potential impact of coupled bred vectors in both ensemble prediction and data assimilation for ENSO predictions. Peña and Kalnay (2004) tested the breeding method for coupled Lorenz models with distinct time scales to mimic the interaction between a slow "coupled tropical ocean-atmosphere system" and an "extratropical atmosphere". They found that breeding is able to isolate the slow modes of the coupled system when rescaling intervals and amplitudes are chosen from physically appropriate scales and the rescaling factor is obtained from the slow component of the system. In contrast, Lyapunov and Singular vectors are unable to isolate the slow modes, because they are based on linear models, and are therefore dominated by the fast modes.

The results with simpler models encourage us to implement the breeding method in a more complicated and complete model, like a CGCM, that includes many types of instabilities, without sacrificing resolution or simplifying model physics. As a first step, we examine in this paper the growing coupled instabilities obtained using breeding in a

fully coupled general circulation model. Our objective is to identify the characteristics of bred vectors associated with the ENSO mode derived from the CGCM and to investigate whether an ENSO-related coupled instability can be isolated from weather noise using the breeding method. Specifically, in this paper, we would like to address the following questions: (1) Can breeding be used to identify the coupled, slowly growing ENSO instability and isolate it from other short term, small scale instabilities such as weather noise? (2) How does the coupled instability evolve with the background ENSO variability? and (3) Are the main characteristics of coupled bred vectors reproducible with two different coupled ocean-atmosphere GCMs?

The structure of the paper is as follows. In section 2, we give a brief description of the NSIPP coupled model, which has been used to generate coupled bred vectors. A brief discussion about the ENSO variability in the NSIPP model is also included in section 2. Section 3 describes how the breeding method is applied in a coupled GCM. Section 4 is devoted to describe the main characteristics of coupled bred vectors derived in the NSIPP model. A comparison of the results obtained from NSIPP and from NCEP/CFS03 is also presented in section 4. A brief summary and discussion of the next phase of our research are included in section 5.

## 2. The NSIPP coupled global circulation model and its ENSO variability

In this study, we test the breeding method on the NSIPP coupled ocean-atmosphere general circulation model, in a perfect model scenario. The NSIPP coupled model is a fully coupled global ocean-atmosphere-land system developed at NASA Goddard Space Flight Center (GSFC) (Miller et al. 2004; Vintzileos et al. 2003). It is comprised of the NSIPP-atmospheric model (AGCM, Bacmeister and Suarez 2003; Bacmeister et al.

2000), the Poseidon ocean model (OGCM, Schopf and Loughe 1995), and the Mosaic land surface model (LSM, Koster and Suarez 1992). The NSIPP AGCM uses a finite-difference C grid in the horizontal and a generalized sigma coordinate in the vertical. An important feature of this AGCM is its inclusion of an empirical cloud diagnostic model and a relaxed Arakawa-Schubert cumulus/boundary-layer parameterization. The OGCM is a Poseidon quasi-isopycnal model designed with generalized horizontal and vertical coordinates. The current NSIPP version uses a reduced-gravity formulation and an embedded surface mixed layer following Sterl and Kaltenberg (1994). The isopycnal region is treated in a quasi-isopycnal fashion, in which layers do not vanish at outcrops and remain a thin minimum thickness at all grid points. The treatment of horizontal mixing within the model is implemented with high order Shapiro filtering. The NSIPP CGCM employs the Goddard Earth Modeling System (GEMS) to couple the atmosphere, ocean and land models. The ocean and atmosphere exchange information once a day. Operational forecasts and hindcasts indicate that forecasts for the Niño3 index[1] remain skillful up to 9 months lead-time, depending on the starting month. Forecast information can be found under http://nsipp.gsfc.nasa.gov/.

A 50-year simulation run has been made with a research version of the NSIPP CGCM identical to the operational model except for a slightly coarser resolution (AGCM: 3.75° in longitude by 3° in latitude and 34 sigma layers; OGCM: 1.25° in longitude by 1/2° in latitude and 27 layers). This integration is referred to as the "control" or "background" run in this paper. The Niño3 index obtained from this control run (not shown) exhibits a realistic ENSO-like variability, although its biennial component is

[1] The Niño3 index is defined as the spatial average of SST anomalies (control) in the Niño3 domain (150°E-90°W; 5°S-5°N). The BV Niño3 index is defined in the same way except that the BV SST perturbations are used instead of SST anomalies.

stronger than observed. In agreement with observations (Boulanger and Menkes 1995, 1999), the control run simulation shows warm anomalies at the thermocline level prior to the SST anomalies. This indicates that air-sea interaction processes and coupled instabilities can be reasonably represented by the CGCM. The spatial patterns of the coupled ENSO variability of the control run are presented in the left panels of Figs. 4-6 and will be discussed together with the presentation of the bred vector spatial structure in Section 4.

## 3. Breeding method with the coupled NSIPP CGCM

We used 10 years of the control run, from model year 2020 to 2029, to perform breeding experiments (discussed in the next section) under a "perfect model scenario", i.e., assuming that the control run is the "truth" (or analysis in a forecast system). The breeding method (Toth and Kalnay 1993, 1996, and 1997) originally developed to "breed" fast growing modes for short-to-medium-range atmospheric ensemble forecasting was implemented in the NSIPP CGCM. The breeding cycle includes the following steps (Fig. 1): (1) add a random perturbation on the initial analysis fields (both oceanic and atmospheric restart files); (2) make a one month forecast (coupled breeding run) starting from the perturbed fields; (3) take the difference between the breeding and the control runs; (4) rescale the difference field (referred to as the "bred vector") to the same size as the initial perturbation; (5) add the rescaled bred vector field to the next analysis field; and (6) repeat steps (2) to (5), adding the coupled bred perturbations onto analysis fields and evolving them with background flow, which forms the "breeding cycle", throughout the 10 years. Thus, bred vectors are perturbations aligning along favorable growing directions, periodically resized and added to the next analysis field in

each of the breeding cycles. Bred vectors are essentially a finite-time, non-linear extension of local Lyapunov vectors, representing the preferred instability directions of the evolving basic flow. Under the "perfect model scenario", the analysis fields are considered to be the truth so that both analysis and forecast fields refer to the same control run.

When the system contains many different types of instabilities, like the coupled ocean-atmosphere model, the initial (or rescaled) perturbation amplitude and the rescaling time interval are the two parameters that can be used to select the type of the instability that shows up in the bred vectors (Toth and Kalnay 1993, 1997; Peña and Kalnay 2004). The BVs consist of perturbations related to instabilities whose saturation amplitude is well above the range of amplitudes allowed, and whose growth rate is largest, since perturbations related to slower-growing instabilities are damped more strongly by the rescaling cycle. For example, convective instabilities will quickly saturate at very small amplitude when breeding in a global atmosphere. A similar situation appears in the instability of a coupled atmosphere-ocean system, but in this case the coupled atmospheric signal that we are seeking has smaller amplitudes than the atmospheric "weather noise". Therefore, choosing an atmospheric measure of the amplitude for the rescaling would not be an effective way of retaining the slower growing coupled perturbations (Peña and Kalnay, 2004). For this reason, the variables we choose to rescale the perturbations should be primarily based on oceanic quantities whose variability is dominant at the seasonal to interannual time scales. Moreover, the rescaling time interval in a breeding cycle plays a crucial role for capturing coupled instabilities corresponding to seasonal to interannual time scales and for isolating them from weather

noise. Choosing a rescaling time interval of one month allows saturation of the fast growing weather noise.

We implemented the breeding method in the NSIPP global CGCM by choosing the period of rescaling as one month and a Niño3 SST root-mean-square norm (RMS), as in Cai et al. (2003) in the Zebiak and Cane model. We chose the RMS SST amplitude within the tropical Pacific domain (15°S-15°N and 120°E-90°W) of 0.085°C, or about 10% of the background SST variability. In the perfect model configuration, the control run is used as both the analysis and the background (first guess). The breeding cycle is simplified by adding the perturbations to the control run, rather than to an analysis, and the bred vectors are the rescaled difference between the perturbed run and the control run. Two independent breeding runs were made starting from two independent random perturbations, which were created by taking the difference between two model states at randomly chosen months. Each run contains 123 months, starting from model year 2019 September to year 2029 December. The starting month is chosen so that the first major warming event takes place about 2 years into the breeding run to ensure the coupled bred modes are closely associated with ENSO. The first three months of the breeding runs are treated as a transient period allowing the bred vectors to grow from random perturbations. The analysis presented below is derived from the remaining 120 breeding cycles (120 months). We found that the two independent 10-year breeding cycles yielded very similar bred vectors (not shown), so that we combine the two bred vector perturbations as a single time series of 20 years to reduce sampling errors. Hereafter, we will refer to the combined bred vectors as BV perturbations.

## 4. Bred vectors in the NSIPP coupled model

### 4.1. Growth rate of coupled bred vectors

Bred vectors represent, by construction, the instabilities that grow on the background flow. An example of the instabilities captured by the coupled bred vectors is shown in Fig. 2, a snapshot of the bred vector SST field (contours) together with the corresponding background SST field (shading) on July 1 of the model year 2024. It shows that the bred vector field has large amplitude along the sharp temperature gradient in the equatorial cold tongue, coinciding with the background waves along the edge of the cold tongue. The bred perturbation seems to suggest that the instability tends to make the waves break. Clearly, the formation of tropical instability waves is captured by the bred vectors. Although the bred vectors may include both coupled and uncoupled ocean instabilities such as those shown in Fig. 2, we illustrate in the remaining part of the paper that a significant portion of the instabilities are related to coupled ENSO dynamics.

The growth rate of the coupled bred vectors is calculated based on the chosen rescaling norm of the perturbation field within the tropical Pacific region:

$$G(t) = \frac{\sqrt{\frac{1}{NG}[BV_{SST}(t)]^2}}{\sqrt{\frac{1}{NG}[BV_{SST}(t-1)]^2}} \qquad (1)$$

where $NG$ is the total number of model grid points in the Niño3 region and $t$ is the model time in months. In other words, we measure the growth rate of bred vectors by their amplification factor within a month. In the 10-year experiment, the typical value of the growth rate in one month of the NSIPP coupled model varies around 3 to 5 (not shown), which is much larger than the coupled instability found by Cai et al. (2003) for the ENSO mode in the ZC model, about 1 to 3 per month. This is to be expected since the growth

rate in the coupled GCM includes both coupled and uncoupled instabilities of any kind, such as the tropical wave instability shown in Fig. 2. We interpret the growth rate of 3-5 per month as consisting of a noisy background growth rate of (mostly uncoupled) instabilities of about 3 per month (a component essentially absent in the ZC model), plus a coupled growth of about 1-2 per month, associated with the ENSO signal that we are seeking.

In order to test whether there is a component of the perturbation growth (above the background noisy growth rate of about 3 per month) evolving upon the coupled ENSO background state (rather than growing randomly), we calculate the lag/lead correlation between the growth rate and the absolute value of the background Niño3 index. We use the absolute value of the Niño3 index in order to account for the large amplitude of both positive and negative SST anomalies. It is evident in Fig. 3 that the growth rate of coupled bred vectors tends to be largest about 3-4 months prior to the time at which the background ENSO amplitude reaches its maximum stage (positive or negative). There is also a relatively weaker growth at about 4 months after the maximum stage of the background ENSO. These results are qualitatively in good agreement with the results obtained with the ZC model in Cai et al. (2003). The results shown here suggest that the breeding method can serve as a natural filter to identify the slow, coupled instability related to ENSO variability by selecting the proper rescaling parameter in the breeding cycle. Therefore, we can expect that projecting the initial perturbations of ensemble members onto ENSO-related growing errors should improve predictions in an ensemble forecast system, as in Cai et al (2003).

### 4.2. The structure of the coupled BV mode

The spatial patterns of the coupled BV can be identified by constructing regression maps for both oceanic and atmospheric variables against the BV Niño3 index, defined as the spatial average of BV SST in the Niño3 domain. This regression filters out perturbations unrelated with ENSO, like the tropical equatorial instability shown in Fig.2. We will compare those maps with the background regression maps constructed with the same regression method but using the background Niño3 index in order to determine whether the coupled BV modes can capture the growing features associated with background ENSO variability.

The oceanic global regression maps for the background fields show the typical tropical variability corresponding to the ENSO mature stage (Fig. 4(a)-(c)). These patterns include a large warming extended from the east to central equatorial Pacific, a deepening thermocline in the eastern equatorial Pacific, and an accompanying shallowing feature off the equator in the western basin, and a basin-wide eastward current anomaly. The regression maps for the BV fields are shown in Fig. 4(d)-(f). The coupled BV mode exhibits a strong signal in the equatorial Pacific and fairly weak variability away from the tropics. The patterns of the coupled BV mode are reminiscent of those in the background state except that the BV mode is more confined to the east and to the equator. This feature is physically meaningful, since it reflects a larger sensitivity to perturbations of the background flow in the shallower thermocline in the east along the equator. It is also consistent with the delayed oscillator theory, which considers that the perturbations grow primarily over the eastern equatorial basin. It is known that in the mean the easterly wind stress is balanced by the zonal pressure gradient, which piles up warm water in the western basin, resulting in a thermocline that slopes down toward the west. The shoaling

thermocline in the east implies that the thermodynamic feedback between SST and near surface ocean variables is much stronger in the east than in the west. As a result, oceanic perturbations in the eastern basin will be easily amplified through positive feedbacks from air-sea interaction.

The atmospheric components of the ENSO mode derived from the control run and the BV field are displayed in Fig. 5. We first examine the tropical Pacific domain to see the direct impact related to boundary heating anomalies. Fig. 5 shows that the patterns in the BV fields have many features in common with the patterns of the background state, namely, westerly wind perturbations located in the central equatorial Pacific and the baroclinic structure in the height fields corresponding to the location of BV SST in Fig 4(d). In addition, the BV outgoing radiation reflects an enhanced convection activity in the eastern basin. These features reinforce the conclusion that the leading coupled BV mode is related to the coupled instability.

It is of interest to point out that the coupled BV also reflects the sensitivities in extratropical regions associated with background ENSO atmospheric teleconnections. Shown in Fig. 6 are the regression maps of surface pressure and geopotential at 200mb in Northern Hemisphere for the background state and for the BV field. The teleconnection patterns of the background state indicate a low-pressure anomaly over the North Pacific and a high-pressure anomaly over North America. This barotropic structure is very robust and extends to a high altitude. It is induced by wave-train patterns associated with the large scale heating in the tropics. For BV maps, strong responses can also be identified in those regions, especially where background regression maps show a strong gradient, for example in the mid Pacific at 30°N and east coast of North America. Wave-

train patterns can also be found in BV regression maps. In the Southern extratropical region (not shown), atmospheric regression maps show a teleconnected pattern associated with background ENSO, and related BV dynamical sensitivities.

In order to show how the coupled BV mode evolves with the background ENSO evolution as in Cai et al. (2003) with the ZC model, we construct lead/lag regression maps against the time series of the amplitude of the background Niño3 index with a lead/lag time up to 6 months (Fig. 7). It is clear that the temporal evolution of the coupled BV mode is highly related to the background ENSO evolution. It shows that in the eastern basin the coupled BV mode leads the large amplitude of the background ENSO events by several months. The signal is clearly coming from the coupled dynamics because an increase of the ocean heat content and a warm SST anomaly in the eastern basin as well as the presence of westerly wind anomalies all lead the background ENSO events by about 2-3 months. This coincides with the timing of the maximum growth of the coupled BV mode which also leads the background ENSO events by 3 months (Fig. 3). It is seen from Fig. 7 that west of 130°W, BV surface height and zonal wind stress exhibits a lag response of the background ENSO of about 3 months. Therefore, using the breeding method, we show that the dominant instability in the NSIPP GCM model is initiated in the eastern basin and that the signal is a coupled instability.

### 4.3. Comparison of the NSIPP and the NCEP/CFS03 Bred Vectors

Similar breeding experiments were carried out with the coupled forecast system model (CFS03) developed in the National Centers for Environmental Prediction (NCEP). The atmospheric component uses the current version of medium range forecast (MRF)

global model with a spectral truncation of 62 waves (T62) in the horizontal (equivalent to nearly 200 Km) and 64 vertical levels in sigma coordinate (Kanamitsu 1989; Kanamitsu et al. 1991; Caplan et al. 1997; Wu et al. 1997). The ocean component is the GFDL Modular Ocean Model V.3 (MOM3) with 40 layers in the vertical (Pacanowski and Griffies, 1998). The zonal resolution is 1° and the meridional resolution is 1/3° between 10°S and 10°N, gradually increasing through the tropics until it is fixed at 1° poleward of 30°S and 30°N.

Two independent breeding experiments were performed by choosing the last 4 years from a 23-year perfect model experiment as the background state. This 4-year period covers a warm event which matures at the model year 21, 2 years into the breeding run. The rescaling factor for perturbations is based on the SST norm in the whole tropical belt (10S-10N) and the perturbation size was chosen as 0.1°C. As in the breeding experiments performed with the NSIPP CGCM, we chose one-month as the rescaling period. Like the NSIPP coupled experiments, the two BV runs for the NCEP system were very similar despite having been started with different random perturbations so that their results are processed as a single 8-year time series. Comparisons between the results from the NSIPP and the NCEP/CFS03 coupled system are made for the purpose of demonstrating the robustness of the bred vectors in coupled GCMs[2].

Fig 8 (a)-(f) are background oceanic regression maps of two coupled GCMs. The oceanic components from the two GCMs successfully produce fundamental features of ENSO. Their differences also reflect differences of numerical schemes in the model dynamics or different choices of physical parameterizations. The meridional structure of

[2] Unfortunately, the experiments performed at NCEP were erased, so that we have only a limited number of diagnostic comparisons available.

warming and thickening surface height (Figs. 8(a)-(b)) in the NCEP/CFS03 GCM in the Eastern Pacific is wider than that of the NSIPP GCM (Figs. 8(d) and (e)). In addition, the regressed surface height of NCEP/CFS03 shows the southern branch of the shoaling patterns off the equator extends more southward instead of being meridionally limited as in the NSIPP case. This can also be seen in the SST and zonal current patterns. Despite those distinctions, the bred vectors from the two coupled systems have significant similarities linked with the background ENSO. To compare BV structures, we show the EOF modes of oceanic variables. Fig. 9(a)-(c) are the first EOF mode of the BV SST and first two modes for the BV thermocline from the NSIPP CGCM and Fig. 9(d)-(f) are the same modes using BV from NCEP/CFS03. Despite the fact that these are two different CGCMs, with very different background evolution, there is a strong resemblance between the BV EOF modes. Both the leading modes (EOF1) in NSIPP and NCEP/CFS03 bred vectors based on SST show an ENSO-associated warm feature in the tropical Eastern Pacific, farther east than in their respective background (not shown). Reflecting the different mean structures and background ENSO variabilities from a different coupled system, the NCEP/CFS03 BV SST EOF1 extends over a larger spatial scale, covering the whole Niño3 domain while the BV SST EOF 1 from NSIPP model is confined to east of 130°W and is meridionally limited. These two EOF1 modes respectively explain 11% and 14% variance from the total growing SST perturbations. This suggests that the coupled growing perturbations associated with ENSO variability represent at least 10% of the total growing perturbations due to a variety of instabilities that appear in a coupled GCM. *The fact that the leading EOF modes from BV fields in both coupled systems show an ENSO-like structure confirms our conjecture that the breeding method is capable of*

*capturing the coupled instability even in the presence of other types of instabilities in the fully coupled GCM model.* Moreover, this mode is robust and dominant. Even if we enlarge the domain for the EOF analysis to a global domain, the same mode appears, showing fairly weak oceanic amplitude in the extra-tropics. This indicates that the breeding method can help to identify the largest growing error projecting on the ENSO variability in a global coupled model and can be applied to a model with full, complete physics such as a GCM, with the full resolution of model output.

Similar natural sensitivities in the eastern Pacific can also be found in the BV thermocline fields of both systems (Figs. 9 (b), (c), (e) and (f)). Both leading EOF modes of the BV thermocline have a deepening feature along the equator and shoaling features off the equator, except that the EOF1 from NCEP/CFS03 extends almost across the whole basin. In addition, both EOF2 modes have a dipole pattern along the equator and establish a wave couplet off the equator in the western basin. All the information above reveals that oceanic perturbations will develop as Kelvin/Rossby wave packages, propagating the upwelling/downwelling signals in the tropical region. It should be noted that the EOF1 of the BV thermocline is close to the EOF1 of BV SST and there is a high correlation between their corresponding leading principal components (not shown). These two modes represent the dominant growing coupled instability, which has been also been obtained by the BV oceanic regression maps. The robustness of the results from two different coupled models supports our hypothesis that bred vectors are associated with the background ENSO variability. The differences between the BVs indicate that bred vectors are sensitive to model behavior. For example, different vertical mixing schemes adopted in ocean models will have an impact on thermocline variations

particularly in the shallow mixed layer region.

Based on the regression maps against with BV Niño3 index (not shown) in the tropical region, we can also deduce that the coupling strengths are different in the two coupled GCMs. In both ocean components, a 1-meter variation (deepening) in BV thermocline corresponds to 0.1 °C warming in the eastern Pacific. The corresponding BV zonal wind stress shows a perturbation of 1.5 $Nm^{-2}$ from the NSIPP AGCM, and it prevails in the central basin. In contrast, the corresponding stress perturbation is only 0.5 $Nm^{-2}$ in NCEP/CFS03 case. In addition, the regressed BV surface pressure and geopotential height for the NCEP/CFS03 model are less organized in the tropics than for the NSIPP coupled model. This seems to suggest that perturbations are more strongly coupled in the NSIPP CGCM in the tropical domain.

There are also similarities between the two systems in the extratropical ENSO-associated teleconnection patterns. Fig. 10(a),(b) are the regression maps of BV surface pressure from the two coupled models. Similar responses can be identified from the eastern basin of the North Pacific to the North Atlantic despite the different responses for other locations. This type of information should be particularly valuable for ensemble forecasting since the robust feature teleconnected to ENSO variability will remain and influence other locations.

## 5. Summary

In this study, we demonstrated for the first time the feasibility of applying the breeding method to a global coupled ocean-atmosphere general circulation model to obtain ENSO coupled instabilities. The results from the BV fields derived from the NSIPP coupled model show that the breeding method is capable of obtaining the fast

growing coupled modes associated with ENSO variability. Potential predictive impact has been shown in the BV growth rate, by the fact that the maximum growth leads the warm/cold event by about three months. Therefore, the growth rate can be viewed as a precursor to background ENSO variability. In particular, the amplitude of the BV in the eastern tropical Pacific increases before the development of the background El Niño events. Therefore, the bred vectors contain ENSO-related perturbations that can be used as the initial perturbations for ensemble forecasting for improving ENSO forecast skill. The three-month lead time in our results (compared with 6-12 months for the ZC model) may seem to be too short for improving current ensemble forecast system. However, we conjecture that this relatively short time-lead is partially due to the fact that the ENSO cycle in this long simulation is more biennial than 3-7 years. This biennial time scale shortens the "growing season" of bred vectors because of the relatively fast pace of the evolving background state. We would expect to obtain a longer lead time from a BV growth rate derived from the NSIPP operational system since it will reflect the real oceanic memory from the observations during initialization, although the shorter time-lag may be also associated with the presence of other weather and oceanic instabilities.

One of the main tasks in our study has been to extract the physical growing mode from the total growing variability, separating its signal from noise associated with weather and other instabilities. We used regression BV maps to illustrate that the ENSO-associated features can be captured by the breeding method. For the oceanic fields, the variability mainly comes from the tropical Pacific and has many features in common with the background ENSO variability. The mean structure makes the eastern equatorial Pacific, with a shallow thermocline, the region of strongest dynamical sensitivity.

Corresponding to the BV oceanic fields, the atmospheric BV response is also reminiscent of the background ENSO features (e.g. a surface pressure anomaly field with a sea-saw pattern from west to east) in the tropical Pacific, indicating that the dominant mode of BV is indeed related to ENSO-associated coupled instabilities. In addition to the coupled characteristics shown in the tropical domain, the extratropical circulation anomalies associated with these coupled BV display a wave-train like teleconnection pattern over the North Pacific and North America. The patterns are known to be strongly teleconnected to ENSO variability.

The robustness of the coupled BV modes has been demonstrated by comparing bred vectors derived from the NSIPP CGCM and NCEP/CFS03 CGCMs. In an EOF analysis applied to BV fields, the leading EOF modes for both systems show similar ENSO-related features (warming/deepening thermocline) in the tropical eastern Pacific, indicating that the leading fast growing mode is due to the ENSO coupled instability. In addition, a strong resemblance between these two independent experiments can be found in many fields, even in those atmospheric teleconnected regions associated with background ENSO development. Our results indicate that the breeding method can serve as a natural filter to isolate the slowly-varying, coupled instabilities in a coupled GCM. Furthermore, global sensitivities associated with the coupled instability initiated from the tropical Pacific can be retained even though the rescaling is simply done in the tropical Pacific.

We conjecture that capturing the coupled bred vectors may benefit data assimilation and ensemble forecasting and improve ENSO prediction skill, as shown in Cai et al (2003) for the ZC model. Therefore, the next stage of our research is to employ these

methods in the NSIPP operational system. In particular, we plan to test whether the ensemble forecasts with coupled BVs as initial perturbations are more effective than current ensembles that use random perturbations introduced in the separate components. Corazza et al (2002) found that in a quasi-geostrophic system, a hybrid 3DVar background error covariance augmented with the inner product of BVs improved the analysis and the forecasts. Similarly, for the coupled system, the BVs should give the structure of the "errors of the month", so that these structures could be used to augment the background error covariance of the current Optimal Interpolation data assimilation scheme and improve the assimilation and forecast of the ENSO-related instabilities.

**Acknowledgements:**

We greatly appreciate many valuable discussions with Max. J. Suarez. We are very grateful to Sonya Kulkarni Miller for much technical support. This work has been supported by grants from the NASA Seasonal to Interannual Prediction Project (NASA-NAG-55825 and NASA-NAG-12418).

**References**

Bacmeister, J. T. and M. J. Suarez, 2002: Wind stress simulations and the equatorial momentum budget in an AGCM. *J. Atmos. Sci.*, 59, 3051-3073.

Bacmeister, J., P. J. Pegion, S. D. Schubert, and M. J. Suarez, 2000: Atlas of Seasonal Means Simulated by the NSIPP I Atmospheric GCM. *NASA/TM-2000-104606*, vol. 17.

Battisti, D. S., 1988: The dynamics and thermodynamics of a warm event in a coupled tropical atmosphere-ocean model. *J. Atmos. Sci.*, 45, 2889-2919.

Bengtsson, L. U. Schleese, E. Roeckner, M. Latif, T. P. Barnett, and N. Garham, 1993: A two tiered approach to climate forecasting, *Science*, **261,** 1026-1029.

Boulanger, J.-P., and C. Menkes, 1995: Propagation and reflection of long equatorial waves in the Pacific and reflection of long equatorial waves in the Pacific Ocean during 1991-1993 El Nino. *J. Geophys. Res.*, **100,** 25041-25059.

___, and C. Menkes, 1995: Long equatorial wave reflection in the Pacific Ocean from TOPES/POSEDON data suring the 1992-1998 period. *Clim. Dyn*, **15,** 205-225.

Busalacchi, A. J., K. Takeuchi, and J. J. O'Brien, 1983: Interannual variability of the equatorial Pacific revisited, *J. Geophys. Res.*, **88,** 7531-7562.

Cai, M., 1995: A simple model for the climatology and ENSO of equatorial Pacific ocean-atmosphere system. *Proceedings of the 20th Annual Climate Diagnostics Workshop, Seattle.* 314-317.

___, 2003: Formation of the Cold Tongue and ENSO in the Equatorial Pacific Basin. *J. Climate*, **16**, 144-155.

___, E. Kalnay, and Z. Toth, 2003: Bred vectors of the Zebiak-Cane Model and their application to ENSO predictions. *J. Climate*, **16**, 40-55.

Cane, M. A., S. E. Zebiak, and S. C. Dolan, 1986: Experimental forecasts of El Niño, *Nature*, **321**, 827-832.

Caplan, P., J. Derber, W. Gemmill, S.-Y. Hong, H.-L. Pan, and D. Parrish, 1997: Changes to the 1995 NCEP operational medium-range forecast model analysis-forecast system. *Wea. Forecasting*, **12**, 581-594.

Chen, D., S. E. Zebiak, A. J. Busalacchi, and M. A. Cane, 1995: An improved procedure for El Niño forecasting, *Science*, **269**, 1699-1702.

Chen, D., M. A. Cane, A. Kaplan, S. E. Zebiak, and D. Huang, 2004: Predictability of El Niño over the past 148 years, *Nature* **428**, 733 – 736.

Chen, Y.-Q., D. S. Battisti, T. N. Palmer, J. Barsugli, and E. S. Sarachik, 1997: Astudy of the predictability of tropical Pacific SST in a coupled atmosphere-ocean model using singular vector analysis: The role of annual cycle and the ENSO cycle. *Mon. Wea. Rev.*, **125**, 831-845.

Corazza, M., E. Kalnay, D. J. Patil, E. Ott, J. A. Yorke, B. R. Hunt, I. Szunyogh and M. Cai, 2002: Use of the breeding technique in the estimation of the background covariance matrix for a quasi-geostrophic model. AMS Symposium on Observations, Data Assimilation and Probabilistic Prediction, pp. 154–157, Orlando, Florida, January 2002.

Dijkstra, H. A. and J. D. Neelin, 1999: Coupled process and the tropical climatology. Part III: Instabilities of the fully coupled climatology. *J. Climate*, **12**, 1630-1643.

Fan, Y., M. R. Allen, D. L. T. Anderson and M. A. Balmaseda, 2000: How predictability depends on the nature of uncertainty in initial conditions in a coupled model of ENSO. *J. Climate*, **13**, 3298-3313.

Jin, F.-F., 1996: Tropical ocean-atmosphere interaction, the Pacific cold tongue, and the El Niño/Southern Oscillation. *Sciences*, **274**, 76-78.

___, 1997: An equatorial ocean recharge paradigm for ENSO. Part I: conceptual model. J. Atmos. Sci., 54, 811-829.

Lau, N. C., 1985: Modelling the seasonal dependence of the atmospheric response to

observed El Niños 1962-1976, *Mon. Wea. Rev.*, **113**, 1970-1996.

Kalnay, E. and Z. Toth, 1994: Removing growing errors in the analysis cycle. Preprints of the AMS 10th Conference on Numerical Weather Prediction, in Portland, OR, July 18-22 1994, pp 212-215.

Kanamitsu, M., 1989: Description of the NMC global data assimilation and forecast system. *Wea. Forecasting*, **4**, 334-342.

___, and Coauthors, 1991: Recent changes implemented into the global forecast system at NMC. *Wea. Forecasting*, **6**, 425-435.

Koster, R. D., and M. J. Suarez, 1992: Modeling the land-surface boundary in climate models as a composite of independent vegetation stands. J. Geophys. Res., 97, 2697.

Miller, S. K., M. M. Rienecker, M. J. Suarez, P. J. Pegion and J. T. Bacmeister, 2004: The GMAO CGCM VI – climatology and interannual variabilitu. NASA/TM-104606.

Rosati, A., K. Miyakoda, and R. Gudgel, 1997: The impact of ocean initial conditions on ENSO forecasting with a coupled model. *Mon. Wea. Rev.*, 125, 754-772

Schopf, P., and Loughe, A., 1995: A reduced-gravity isopycnal ocean model: hindcasts of El Niño. *Mon. Wea. Rev.*, **123**, 2839-2863.

Sterl, A., and A. Kaltenberg, 1994: Embedding a mixed layer model into a ocean general circulation model of the Atlantic: The importance of surface mixing for heat flux and temperature. *J. Geophys, Res.*, **99**, 14,139-14,157.

Stockdale, T. N., D. L. T. Anderson, J. O. S. Alves, and M. A. Balmaseda, 1998: Global seasonal rainfall forecasts using a coupled ocean-atmosphere model. *Nature*, **392**, 370-373.

Suarez, M., 1996: Dynamical aspects of climate simulations using the GEOS general

circulation model, *NASA Technical Memorandum 104606*, **10**, p77.

Toth, Z. and E. Kalnay, 1993: Ensemble forecasting at NMC: the generation of perturbations. *Bull. Amer. Meteor. Soc.*, **74,** 2317-2330.

___ and ___, 1997: Ensemble forecast at NCEP and the breeding Method. *Mon. Wea. Rev.*, **125,** 3297-3319.

Vintzileos, A., M. M. Rienecker, M. J. Suarez, S. K. Miller, P. J. Pegion and J. T. Bacmeister, 2003: Simulation of the El Niño-Interannual Prediction Project coupled general circulation model. *CLIVER Exchanges*, **8** (4), 25-27.

Van der Vaart, P. C. F., H. A. Dijkstra, and F-F Jin, 2000, The Pacific cold tongue and the ENSO mode: A unified theory within the Zebiak-Cane model. *J. Atmos. Sci.*, **57**, 967—988.

Wu, W., M. Iredell, S. Saha, and P. Caplan, 1997: Changes to the 1997 NCEP operational MRF model analysis/forecast system. *NCEP Technical Procedures Bulletin*, **443**.

Xue, Y., M. A. Cane and S. E. Zebiak, 1997a: Predictability of a coupled model of ENSO using singular vector analysis. Part I: Optimal growth in seasonal background and ENSO cycles. *Mon. Wea. Rev*, **125**, 2043-2056.

___, ___, and ___, 1997b: Predictability of a coupled model of ENSO using singular vector analysis: Part II: Optimal growth and forecast skill. . *Mon. Wea. Rev.*, **125**, 2057-2073.

Zebiak, S. E. and M. A. Cane, 1987: A model El Niño-Southern Oscillation, *Mon, Wea. Rev.*, **115,** 2262-2278.

**Figure Captions**

**Figure 1** Schematic diagram showing a continuously evolving breeding cycle upon the unperturbed (control) model integration in a perfect model setting. The difference between the unperturbed and perturbed forecasts yields the bred vectors. The growth rate is computed as the ratio of the final to the initial size.

**Figure 2** A snapshot of SST in Eastern Pacific showing the bred vectors perturbation (contours: CI = 0.15 °C) evolving with the background flow (shading with an interval of 1°C from 21°C to 30°C) on July 1 of the model year 2024. The dotted contours of the BV indicate negative values.

**Figure 3** Lead/lag correlations between the BV growth rate and the absolute value of the background Niño3 index.

**Figure 4** Oceanic regression maps in the global domain. Left panels are the background fields and right panels the BV fields. (a) SST anomaly (°C); (b) Z20 anomaly (m); (c) surface zonal current anomaly ($ms^{-1}$); (d) BV SST (°C); (e) BV Z20 (m); and (f) BV surface zonal current ($ms^{-1}$). Background fields are regressed with the background Niño3 index and BV fields regressed with the BV Niño3 index. The scales of BV fields are arbitrary but the ratio among BV variables (both oceanic and atmospheric variables) is retained as in the original BV fields.

**Figure 5** The same as Figure 4 except for the atmospheric regression maps over the equatorial Pacific basin. (a) wind field anomaly at 850mb ($ms^{-1}$); (b) surface pressure anomaly (mb); (c) geopotential anomaly at 200mb ($m^2s^{-2}$); (d) outgoing long wave radiation ($Wm^{-2}$); (e) BV wind field at 850mb ($ms^{-1}$); (f) BV surface pressure (mb); (g) BV geopotential at 200mb ($m^2s^{-2}$); and (h) BV outgoing long wave radiation ($Wm^{-2}$).

**Figure 6** The same as Figure 4 except for atmospheric regression maps over the Pacific portion of the Northern Hemisphere. (a) background surface pressure anomaly (mb); (b) background geopotential anomaly at 200mb ($m^2s^{-2}$); (c) BV surface pressure (mb); and (d) BV geopotential at 200mb ($m^2s^{-2}$).

**Figure 7** Lead/Lag regression maps along the equator for BV oceanic fields against the absolute value of the background Niño3 index. (a) SST ($^{\circ}C$); (b) surface height (m); and (c) zonal wind stress ($Nm^{-2}$). The contours are arbitrary but the ratio among BV variables is retained as in the original BV fields.

**Figure 8** Background oceanic regression maps for two coupled GCMs in the tropical Pacific domain. Left panels are the NSIPP anomalies of NSIPP and the right panels the NCEP/CFS03 anomalies. (a) NSIPP SST (°C); (b) NSIPP surface height (m); (c) NSIPP surface zonal current ($ms^{-1}$); (d) NCEP SST (°C); (e) NCEP surface height (m); and (f) NCEP surface zonal current ($ms^{-1}$). The regression maps of NSIPP (NCEP) fields are computed using the NSIPP (NCEP) Niño3 index, respectively.

**Figure 9** The leading EOFs of the BV SST and Z20 perturbations derived from the NSIPP and NCEP/CFS03 CGCMs. (a) EOF1 of NSIPP BV SST; (b) EOF1 of NSIPP BV Z20; (c) EOF2 of NSIPP BV Z20; (d) EOF1 of NCEP BV SST; (e) EOF1 of NCEP BV Z20; and (f) EOF2 of NCEP BV Z20. The scale is arbitrary.

**Figure 10** Atmospheric regression maps of BV 500mb geopotential height in in the Northern Hemisphere (m). (a) for NSIPP and (b) for NCEP/CFS03. Both fields are computed against their own BV Niño3 indices.

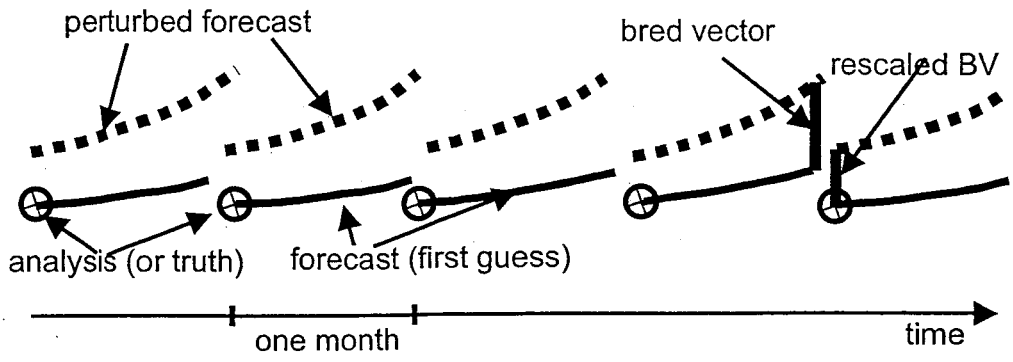


Figure 1 Schematic diagram showing a continuously evolving breeding cycle upon the unperturbed (control) model integration in a perfect model setting. The difference between the unperturbed and perturbed forecasts yields the bred vectors. The growth rate is computed as the ratio of the final to the initial size.

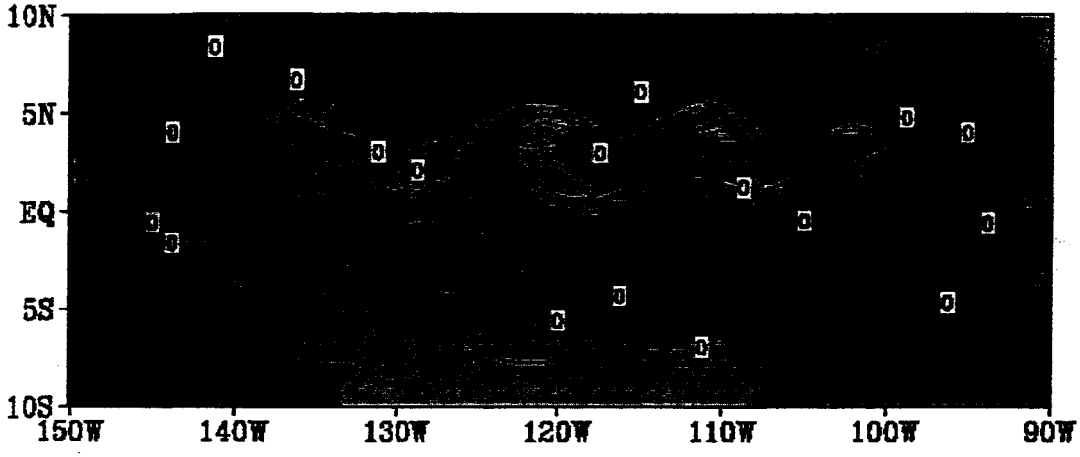


Figure 2 A snapshot of SST in Eastern Pacific showing the bred vectors perturbation (contours: CI = 0.15 °C) evolving with the background flow (shadings with an interval of 1°C from 21°C to 30°C) on July 1 of the model year 2024. The dotted contours of the BV indicate negative values.

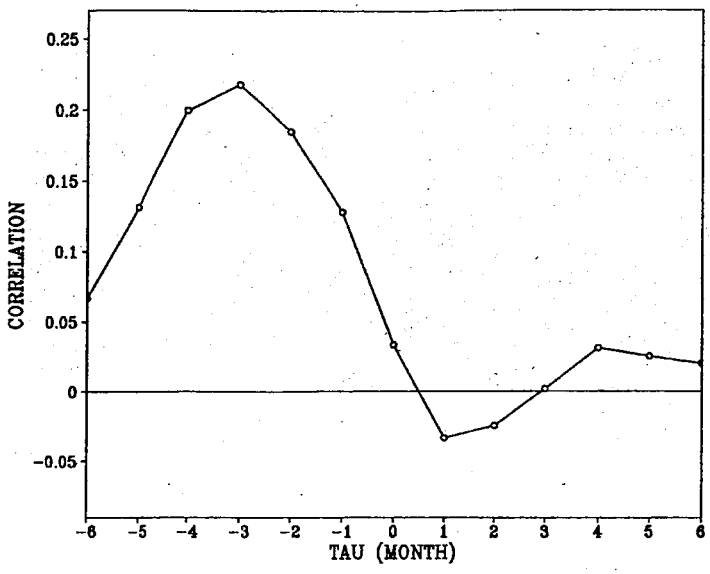


Figure 3 Lead/lag correlations between the BV growth rate and the absolute value of the background Niño3 index.

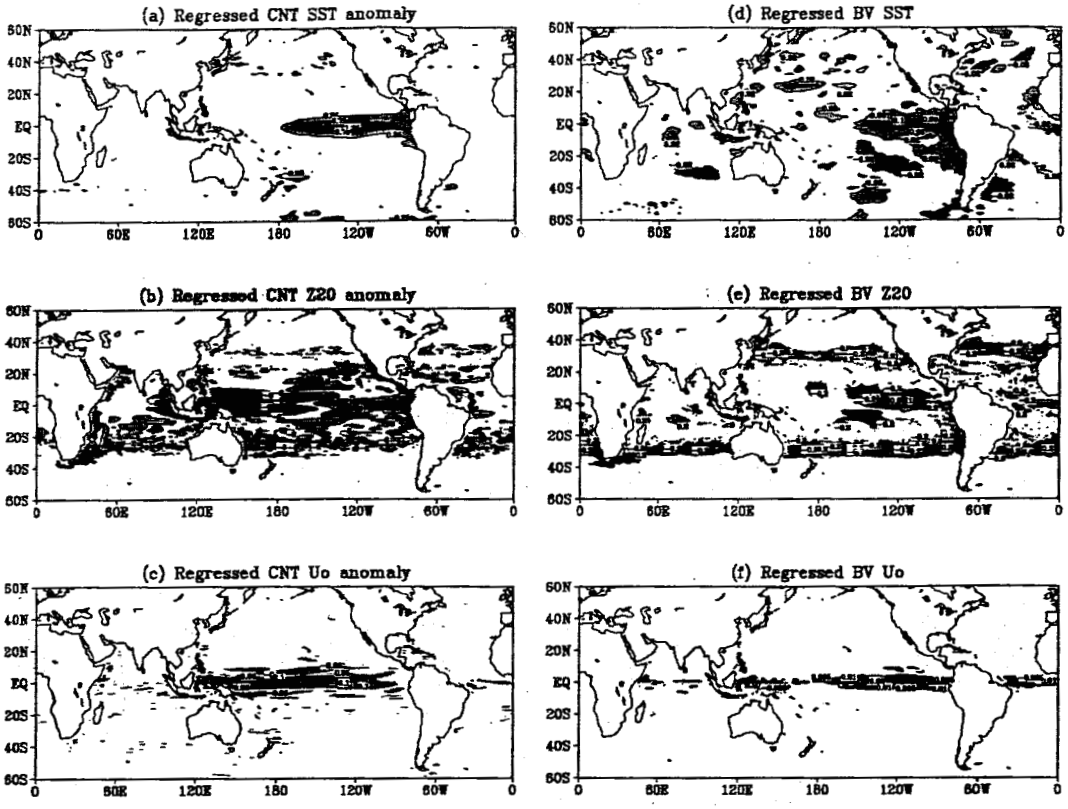


Figure 4 Oceanic regression maps in the global domain. Left panels are the background fields and right panels the BV fields. (a) SST anomaly (°C); (b) Z20 anomaly (m); (c) surface zonal current anomaly ($ms^{-1}$). (d) BV SST (°C); (e) BV Z20 (m); and (f) BV surface zonal current ($ms^{-1}$). Background fields are regressed with the background Niño3 index and BV fields regressed with the BV Niño3 index. The scales of BV fields are arbitrary but the ratio among BV variables (both oceanic and atmospheric variables) is retained as in the original BV fields.

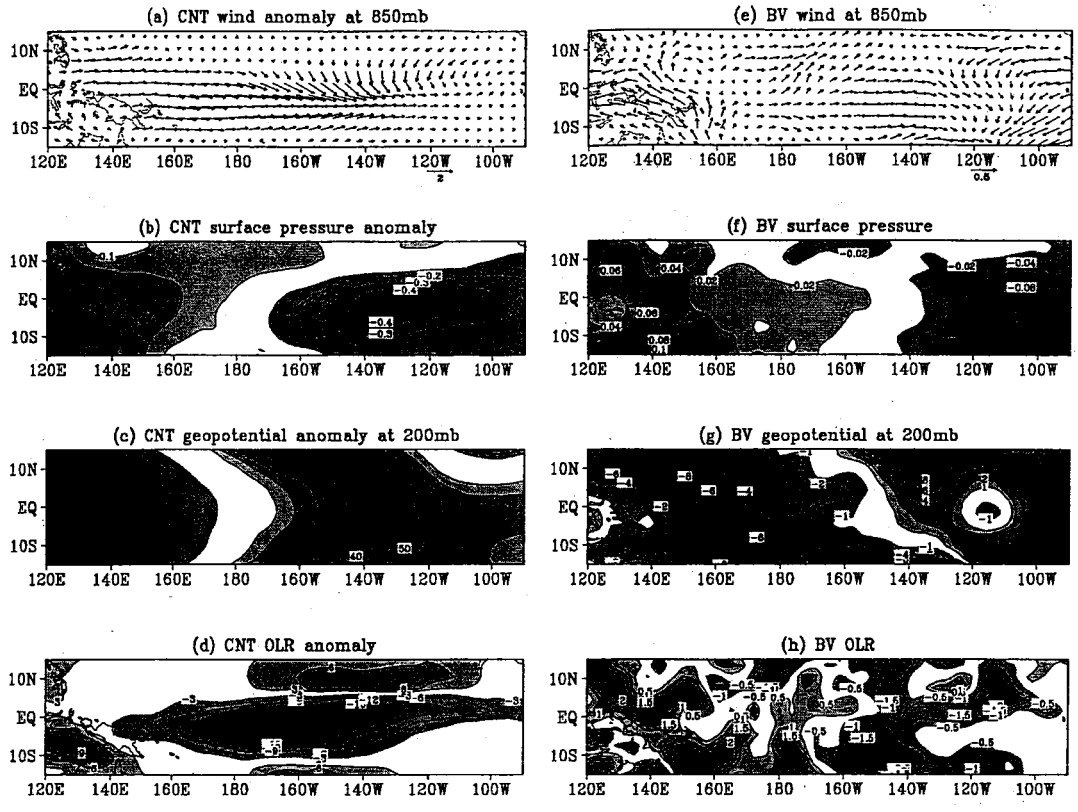


Figure 5 The same as Figure 4 except for the atmospheric regression maps over the equatorial Pacific basin. (a) wind field anomaly at 850mb ($ms^{-1}$); (b) surface pressure anomaly (mb); (c) geopotential anomaly at 200mb ($m^2s^{-2}$); (d) outgoing long wave radiation ($Wm^{-2}$); (e) BV wind field at 850mb ($ms^{-1}$); (f) BV surface pressure (mb); (g) BV geopotential at 200mb ($m^2s^{-2}$); and (h) BV outgoing long wave radiation ($Wm^{-2}$).

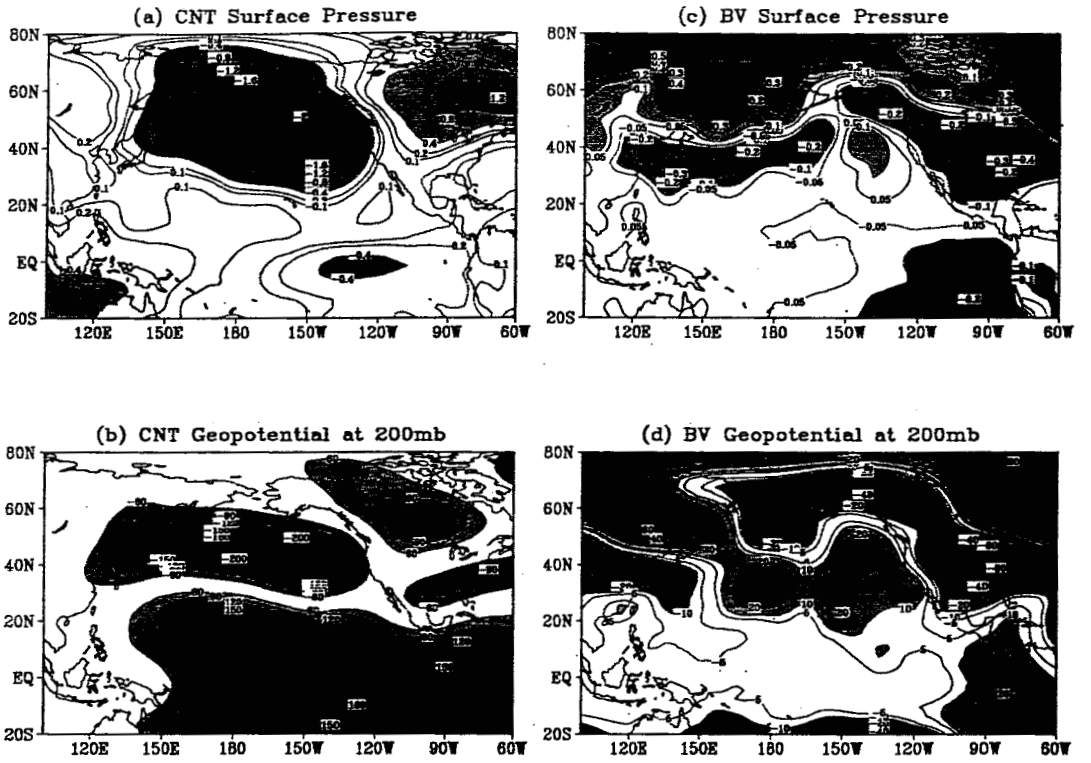


Figure 6 The same as Figure 4 except for atmospheric regression maps over the Pacific portion of the Northern Hemisphere. (a) background surface pressure anomaly (mb); (b) background geopotential anomaly at 200mb ($m^2s^{-2}$); (c) BV surface pressure (mb); and (d) BV geopotential at 200mb ($m^2s^{-2}$).

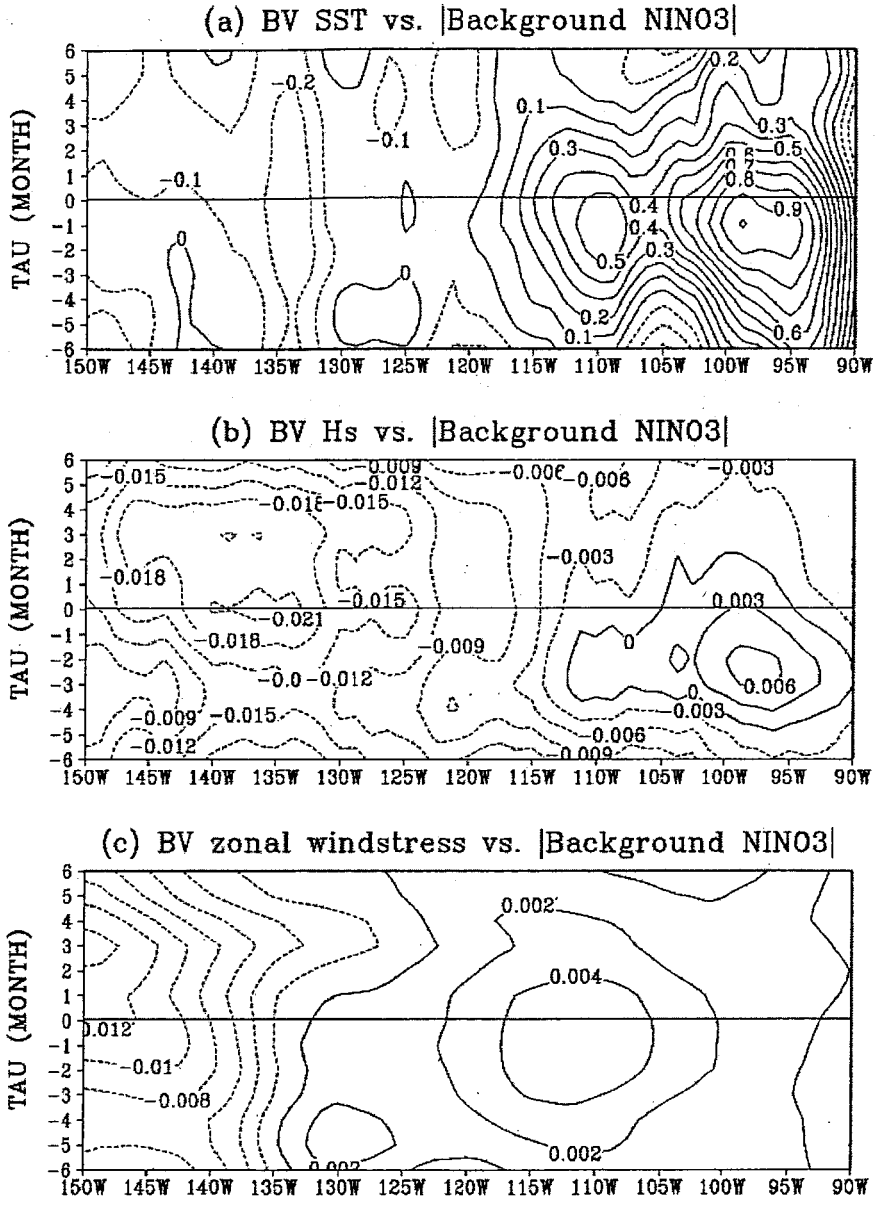


Figure 7 Lead/Lag regression maps along the equator for BV oceanic fields against the absolute value of the background Niño3 index. (a) SST (°C); (b) surface height (m); and (c) zonal wind stress ($Nm^{-2}$). The contours are arbitrary but the ratio among BV variables is retained as in the original BV fields.

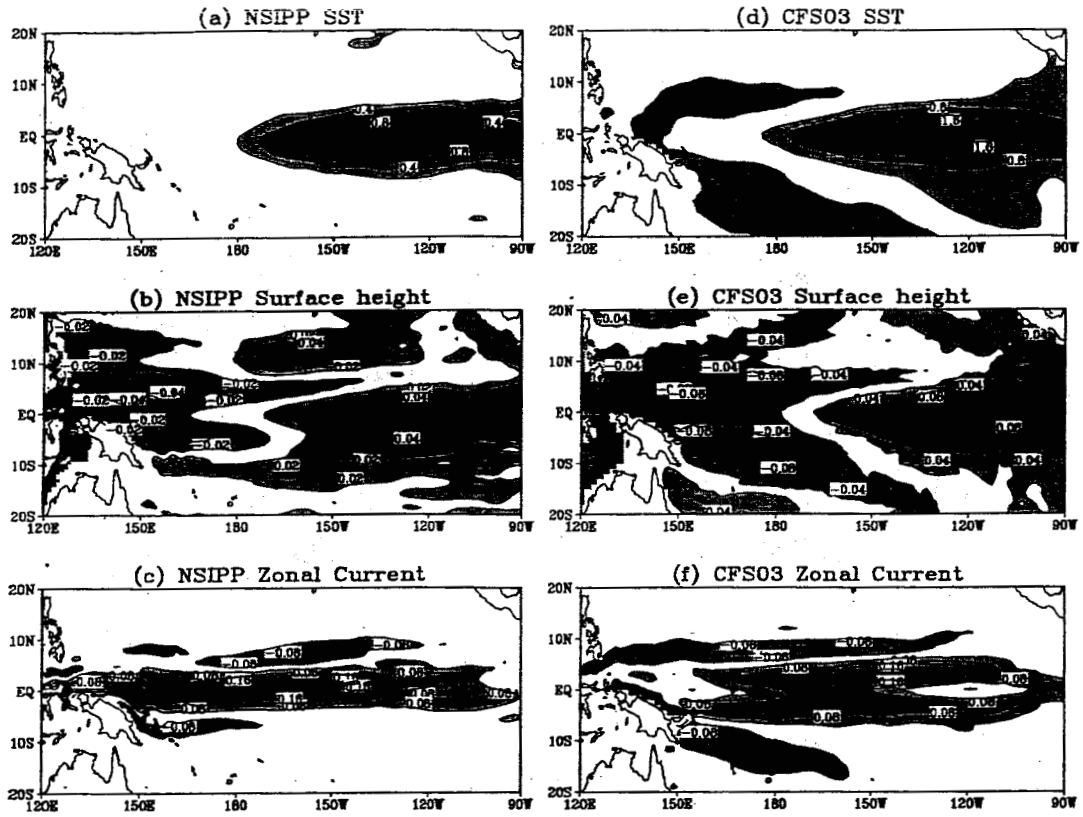


Figure 8 Background oceanic regression maps for two coupled GCMs in the tropical Pacific domain. Left panels are the NSIPP anomalies and the right panels the NCEP/CFS03 anomalies. (a) NSIPP SST (°C); (b) NSIPP surface height (m); (c) NSIPP surface zonal current ($ms^{-1}$); (d) NCEP SST (°C); (e) NCEP surface height (m); and (f) NCEP surface zonal current ($ms^{-1}$). The regression maps of NSIPP (NCEP) fields are computed using the NSIPP (NCEP) Niño3 index, respectively.

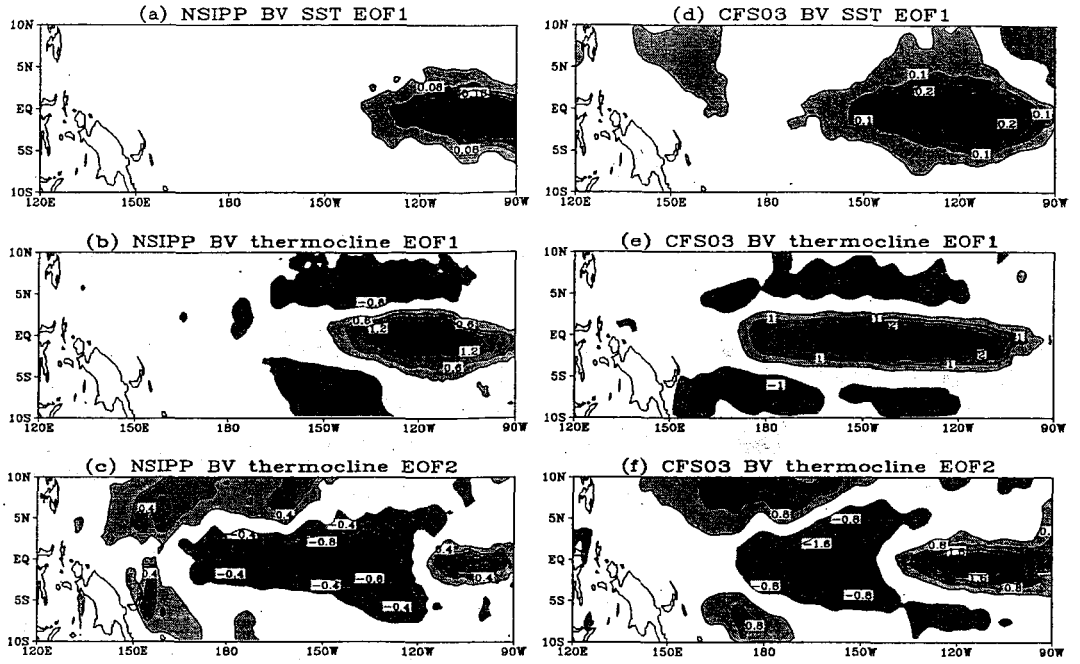


Figure 9. The leading EOFs of the BV SST and Z20 perturbations derived from the NSIPP and NCEP/CFS03 CGCMs. (a) EOF1 of NSIPP BV SST; (b) EOF1 of NSIPP BV Z20; (c) EOF2 of NSIPP BV Z20; (d) EOF1 of NCEP BV SST; (e) EOF1 of NCEP BV Z20; and (f) EOF2 of NCEP BV Z20. The scale is arbitrary.

(a) NSIPP regressed BV 500mb geopotential height

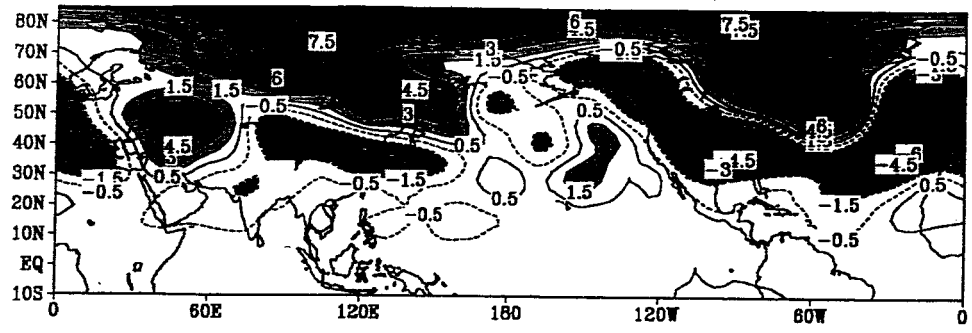


(b) CFS03 regressed BV 500mb geopotential height

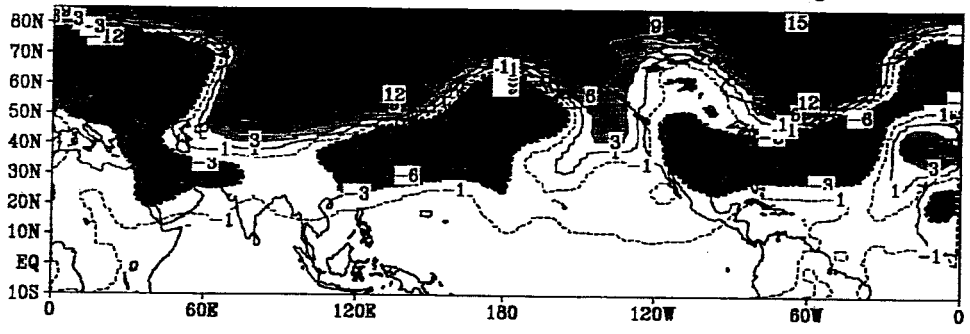


Figure 10 Atmospheric regression maps of BV 500mb geopotential height in in the Northern Hemisphere (m). (a) for NSIPP and (b) for NCEP/CFS03. Both fields are computed against their own BV Niño3 indices.